Appl. Phys. B 80, 817–821 (2005)
DOI: 10.1007/s00340-005-1809-2

Applied Physics B
Lasers and Optics

R.F. OULTON[1,✉]
P.N. STAVRINOU[2]
G. PARRY[2]

Optical coherence of planar microcavity emission

[1]Centre for Process Systems Engineering, Imperial College, London, UK
[2]Centre for Electronic Material and Devices, Imperial College, London, UK

Received: 5 January 2005 / Revised version: 9 March 2005
Published online: 3 May 2005 •

ABSTRACT An analytical expression for the self-coherence function of a microcavity and a partially coherent source is derived. Excellent agreement is found between the model and the experimental measurements from two resonant-cavity light-emitting diodes. The variation of coherence length as a function of numerical aperture is examined and indicates that the variable coherence properties of planar microcavities are determined by the underlying coherences of the microcavity and the source. Furthermore, coherence-length variations approaching a factor of five can be achieved by engineering the cavity finesse.

PACS 85.60.Bt; 42.25.Kb; 85.60.Jb

1 Introduction

The last two decades have seen widespread interest of optical microcavities in both experimental physics and commercial applications [1–3]. Microcavity devices such as resonant-cavity light-emitting diodes (RCLEDs) [2] use the planar microcavity geometry to increase the extraction efficiency of spontaneous emission from materials with high dielectric constants [3]. More recently, microcavities have been used to spectrally and spatially isolate quantum-dot emitters to increase the efficiency of single-photon production [4, 5].

Recent work on planar microcavities has identified the dependence on numerical aperture (NA) of emission properties such as spectral line width [6, 7] and coherence length [8]. The experiments of Birkner and co-workers [9], showing the variations of emission noise as a function of NA, also highlight the intriguing statistical variations in these devices. In the light of these observations, the general variable coherence properties of planar microcavities are the focus of the current letter. Moving between the coherence and spectral domains is trivial due to their implicit Fourier relationship; however, some care must be taken in distinguishing the spontaneous-emission lifetime and the coherence time of a light source. The term coherence is usually associated with the statistics of a group of emitters, whereas the spontaneous-emission lifetime relates to homogeneous groups or individual emitters. Here, the statistical effects of semiconductor quantum well light sources are relevant, since well-width variations, phonon interactions and the process of carrier injection imply inhomogeneous exciton recombination [10, 11].

The coherence time (or length) defines the scale over which mutual interference of a light source can occur. Applications such as low-coherence interferometry, for non-invasive medical imaging [12] (also known as optical coherence tomography), and optical time domain reflectometry (OTDR), for ranging measurements in optical components [13] and surface mapping in integrated circuits [14], rely on the coherence of a source being both large enough to examine detail on the relevant length scale yet small enough to eliminate coherent reflections from distant objects. Here, a light source's coherence effectively determines the detection band for optical time of flight measurements. The variable coherence properties of RCLEDs [8] potentially make them ideal as a light source for applications where a range of length scales must be analysed where, previously, multiple light sources would have been required.

This letter examines the variable coherence of emission from RCLEDs operating at 650 nm and indicates methods by which this aspect of commercial devices could be engineered. Note that although results concerning specific RCLEDs are analysed here, the findings should be applicable to planar microcavity devices in general.

2 Theoretical approach

2.1 *Coherence model of an emitter within a microcavity*

The self-coherence function of an emitter, $\Gamma_{\mathrm{E}}(\tau)$, defined in Born and Wolf [15], can be written as

$$\Gamma_{\mathrm{E}}(\tau) = \int_{-\infty}^{\infty} E(t)E^{*}(t-\tau)\,\mathrm{d}t. \tag{1}$$

Within a cavity, the coherence of a light source is modified on the scale of the cavity coherence time. A first-principles derivation of $\Gamma(\tau, \theta_{\mathrm{c}})$, the self-coherence function of a combined emitter and microcavity system, is cumbersome and too detailed to describe here. However, it can be derived indirectly using a key spectral domain result: the emission intensity from a microcavity system in the weak-coupling regime is given by

✉ Fax: +44-20-7594-6606, E-mail: r.oulton@imperial.ac.uk

the spectral overlap of the optical transfer function of the bare cavity, $H(\omega, \theta_c)$, which is a function of the angle relative to the emission region, θ_c, and the spectral distribution of the underlying source $|E(\omega)|^2$, which is assumed here to be isotropic and polarization independent [16, 17]:

$$I(\omega, \theta_c) = H(\omega, \theta_c) \mid E(\omega)|^2. \tag{2}$$

$\Gamma(\tau, \theta_c)$ can therefore be written as a convolution expression following the Fourier relationship with a spectral distribution function, $I(\omega, \theta_c)$, by the Wiener–Khintchine theorem [15]:

$$\Gamma(\tau, \theta_c) = \Gamma_0 \int_{-\infty}^{\infty} \Gamma_E(\tau - t)\Gamma_C(t, \theta_c)\, dt. \tag{3}$$

Here, $\Gamma_E(\tau)$ is the self-coherence function of the emitter and $\Gamma_C(\tau, \theta_c)$ is the self-coherence function of the cavity. These expressions are both Fourier transforms of the emission spectrum $|E(\omega)|^2$ and the optical transfer function of the bare cavity $H(\omega, \theta_c)$, respectively.

Here, the coherence functions are normalized such that Γ_0 is the peak of the microcavity response in the spectral domain for an emitter tuned to the cavity resonance at ω_t and an angle θ_t:

$$\Gamma_0 = \frac{T_F(\omega_t, \theta_t)(1 + \sqrt{R_B(\omega_t, \theta_t)})^2}{(1 - \sqrt{R_F(\omega_t, \theta_t)R_B(\omega_t, \theta_t)})^2}. \tag{4}$$

Here, $T_F(\omega_t, \theta_t)$ and $R_F(\omega_t, \theta_t)$ are the transmission and reflectivity of the front cavity mirror and $R_B(\omega_t, \theta_t)$ is the reflectivity of the back mirror on resonance. The spectral domain response of the microcavity and emitter is best described using Fig. 1. Here, the peak responses of the bare cavity and emission spectrum are represented in a two-dimensional projection of k-space: the angle-insensitive emitter traces a spherical shell of states of radius $k_E \propto \omega_E$ while the cavity traces a plane of states imposed by the resonance condition $k_z(\theta_c) =$ constant. In general, the frequency of the emitter, ω_E, and the bare cavity, $\omega_c(\theta_c)$, are detuned by $\Delta\omega(\theta_c)$ and are dependent on the angle θ_c. The coupled system is in resonance when $\Delta\omega(\theta_t) = 0$. In the design of these devices, the detuning corresponds to the value at $\theta_c = 0$. Note that in air, only a cone of k-space states are accessible. A more detailed description of this can be found in Ref. [7].

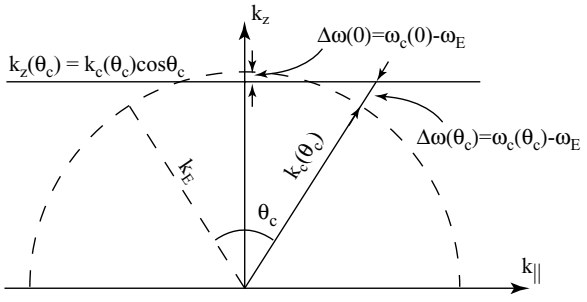

FIGURE 1 Representation of bare microcavity and emission states in k-space

2.2 *Analytical formula for the self-coherence function*

Consider now the functional form of the coherence functions in Eq. (3). The underlying emission spectrum is assumed to be Lorentzian in nature, corresponding to exponential decay in the time domain. Similarly, the transfer function of the cavity, $H(\omega, \theta_c)$, can also be approximated by a Lorentzian close to a longitudinal mode at $\omega_c(\theta_c)$ as the free spectral range is much greater than the spectral width of the source.

$$\Gamma(\tau, \theta_c) = \Gamma_0 \int_{-\infty}^{\infty} \frac{\exp\left(i\omega_E(\tau - t) - \mid \tau - t \mid /\tau_E\right)}{2\tau_E} \times \frac{\exp\left(i\omega_c(\theta_c)t - \mid t \mid /\tau_c(\theta_c)\right)}{2\tau_c(\theta_c)}\, dt. \tag{5}$$

Here, τ_E and $\tau_c(\theta_c)$ are the coherence times of the underlying source and cavity resonances, respectively. Note that τ_E and ω_E are constant with emission angle. The definite integral of Eq. (5) can be evaluated for $\tau > 0$.

$$\Gamma(\tau > 0, \theta_c) = \frac{\Gamma_0}{2\tau_E\tau_c(\theta_c)} \times \left\{ \frac{\tau_c(\theta_c)\Gamma_C(\tau, \theta_c)}{i\Delta\omega(\theta_c) + K(\theta_c)} - \frac{\tau_c(\theta_c)\Gamma_C(\tau, \theta_c)}{i\Delta\omega(\theta_c) + K'(\theta_c)} + \frac{\tau_E\Gamma_E(\tau)}{i\Delta\omega(\theta_c) + K'(\theta_c)} - \frac{\tau_E\Gamma_E(\tau)}{i\Delta\omega(\theta_c) - K(\theta_c)} \right\}. \tag{6}$$

Here, $K(\theta_c) = 1/\tau_c(\theta_c) + 1/\tau_E$ and $K'(\theta_c) = 1/\tau_c(\theta_c) - 1/\tau_E$. The expansion of the integral in Eq. (5) for $\tau < 0$ gives $\Gamma(\tau < 0, \theta_c) = \Gamma^*(\tau > 0, \theta_c)$, which is a consequence of the real-valued spectral density function of Eq. (2).

2.3 *Limiting cases of the self-coherence function*

Examination of Eq. (6) also highlights the correct asymptotic response: if $\tau_c(\theta_c) \gg \tau_E$ then $\Gamma(\tau, \theta_c) \propto \Gamma_C(\tau, \theta_c)$, the coherence function of the cavity. For this condition $K \simeq -K' \simeq 1/\tau_E$ such that

$$\Gamma(\tau, \theta_c) = \Gamma_0 \frac{(1/\tau_E)^2}{\Delta\omega(\theta_c)^2 + (1/\tau_E)^2}\Gamma_C(\tau, \theta_c). \tag{7}$$

Here, the coherence properties are determined by the cavity while the emitter defines a spectral envelope with detuning. Conversely, if $\tau_E \gg \tau_c(\theta_c)$ then $\Gamma(\tau, \theta_c) \propto \Gamma_E(\tau)$, the coherence function for the underlying emission. For this condition $K \simeq K' \simeq 1/\tau_c(\theta_c)$ such that

$$\Gamma(\tau, \theta_c) = \Gamma_0 \frac{(1/\tau_c(\theta_c))^2}{\Delta\omega(\theta_c)^2 + (1/\tau_c(\theta_c))^2}\Gamma_E(\tau). \tag{8}$$

In this case, the coherence properties are determined by the emitter and the spectral envelope by the cavity. In the former case the cavity filters the statistical fluctuation of the emitter. In the latter case the statistical properties of the emitter are extracted intact close to the tuning angle.

3 Analysis of experimental and theoretical results

In the following analysis, the coherence length, $L_c(\theta_a)$, defined in Eq. (9), is used to study the correspondence of spectral domain measurements and the coherence model developed here. Note that the experimental measurements correspond to angles measured in air, θ_a,

$$L_c^2(\theta_a) = c^2 \frac{\int_{-\infty}^{\infty} \tau^2 \mid \Gamma(\tau, \theta_c) \mid^2 \mathrm{d}\tau}{\int_{-\infty}^{\infty} \mid \Gamma(\tau, \theta_c) \mid^2 \mathrm{d}\tau}. \quad (9)$$

For RCLEDs, $\tau_c(\theta_c) > \tau_E$; however, the difference is not large enough to warrant one of the limiting cases of Eq. (6) discussed above. In the following the coherence model is compared with the angle-resolved spectra of tuned and detuned RCLEDs operating near 650 nm. The details of these experiments can be found in Ref. [7]. In summary, the emission spectra for the two devices were recorded for a range of angles using an angular resolving experiment. The devices were fixed to a rotation stage. The emission at each angle was collected through a pinhole situated far from the devices by a monchromator with a spectral resolution of < 1 nm. The pinhole subtended a half angle of $< 0.2^\circ$ at the device, corresponding to a sampling NA $< 10^{-2}$. In addition, the spectra of both devices were measured for NA $= 1$ in an integrating sphere. The coherence functions are determined by inverse Fourier transformation of the angle-resolved spectra, from which the coherence lengths could be calculated using Eq. (9). The model was fitted to the experimental results by optimizing a least-squares objective function, where τ_c, τ_E and $\Delta\omega(0)$ were the fitting parameters. Here, τ_c was assumed to be approximately constant with angle.

3.1 *Variation of coherence length for angle-resolved measurements*

Figure 2 shows the variation of coherence length, $L_c(\theta_a)$, for the tuned (Fig. 2a) and detuned (Fig. 2b) samples. The solid lines represent the best fit for the limiting case of $\tau_c \gg \tau_E$. Overall, the correspondence of experiment and theory is excellent for the lower angles. At large angles, systematic deviation from the model is observed. The minima of the coherence deviation occur at 50° and 65° in the tuned and detuned devices, respectively, which correspond to the same wavelength. The deviation could therefore be attributed to a range of factors such as loss within the doped regions of the RCLEDs or interference due to the various layers that make up the cavity region, where homogeneous approximations have been used in the model.

Table 1 shows the fitting parameter values for the RCLED samples in terms of coherence time and spectral wavelength.

Parameter	Tuned	Detuned
τ_c	0.115 ps (3.89 nm)	0.111 ps (4.04 nm)
τ_E	0.034 ps (13.23 nm)	0.035 ps (12.77 nm)
$\Delta\omega(0)$	(+0.58 nm)	(−5.50 nm)

TABLE 1 Table of fitting parameter values given for both coherence and spectral domains

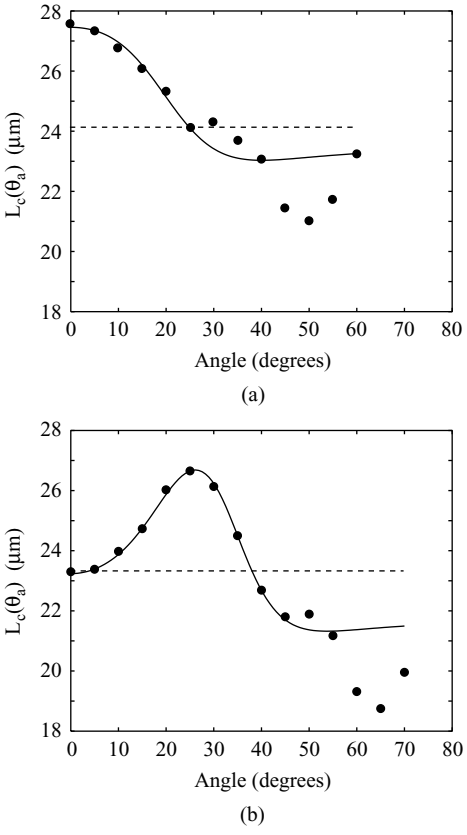

FIGURE 2 Comparison of experimental and model results for coherence-length variation with observation angle for **a** a tuned RCLED and **b** a detuned RCLED

The results are very encouraging on two counts: they corroborate the identical designs of underlying cavity and emitter and infer the design detunings of 0 nm and −6 nm. The trends of fitted data also confirm this by the peak in coherence length at the tuning frequency and angle, which is only clear in the case of the detuned RCLED at approximately 26° or at a detuning of −5.5 nm.

3.2 *Variation of coherence length as a function of NA*

Notice that, at low NAs, when only a few of the transverse cavity modes are sampled, the coherence length is near to that of the bare cavity, $c\tau_c = 34.50\,\mu$m. In this case, statistical fluctuations within the cavity are small since the cavity samples the emission source over a longer time period than its coherence time. This general behaviour is also seen at other sampled emission angles as the cavity lifetime is constant with angle. However, the emission frequency does change with angle: at large NAs, the sampled emission is reconstituted spectrally, reproducing to some extent the underlying statistical fluctuations with a coherence length of $c\tau_E = 10.50\,\mu$m. This appears to be a fair description given the observations of recent experiments [7, 8]. Consider, therefore, the reconstitution of the angle-resolved coherence functions into a coherence function for a given NA. Here, the density of off-axis states and the differential change in solid angle must be considered. Equation (6) is now integrated over

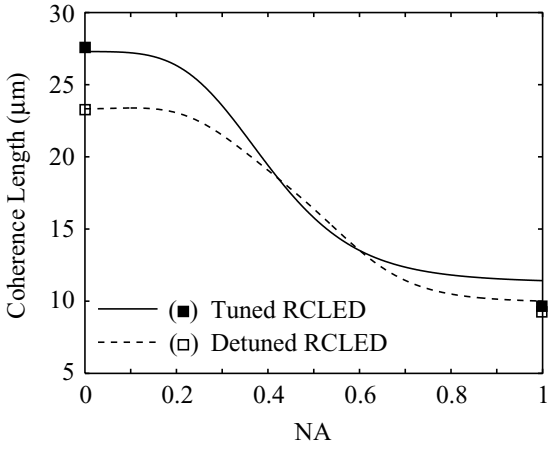

FIGURE 3 Coherence-length variation as a function of NA generated using the fitting parameters in the coherence model for tuned and detuned RCLEDs. Markers at NA extrema denote experimental points determined by measurements at low NA and from an integrating sphere

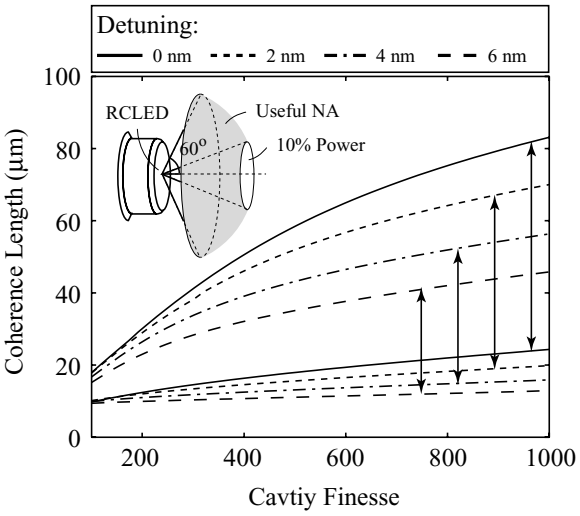

FIGURE 4 Predictions of maximum and minimum coherence as a function of microcavity finesse and detuning with respect to the emission source across the useful emission NA. The diagram in the *top left corner* illustrates the useful NA

solid angle up to a specific NA $= \sin\theta_a$.

$$\Gamma(\tau, \mathrm{NA}) = \int_0^{2\pi}\int_0^{\theta_a} \Gamma(\tau, \theta_c)\frac{\mathrm{d}\Omega_c}{\mathrm{d}\Omega_a}\,\mathrm{d}\Omega_a = 2\pi\int_0^{\theta_a} \Gamma(\tau, \theta_c)\frac{\cos\theta_a}{\cos\theta_c}\sin\theta_a\,\mathrm{d}\theta_a. \quad (10)$$

Figure 3 shows the variation of coherence length as a function of NA for the two RCLEDs under investigation evaluated using the coherence model with the parameters shown in Table 1. Although experimental results for these trends are not available, they do follow the generic trend observed recently in a 4-nm device by interference measurements of Ref. [8]. The square markers show the coherence-length extrema calculated from measured spectra at normal incidence and NA = 1 in an integrating sphere, which closely correspond to the coherence lengths of the bare cavity, $c\tau_c$, and the underlying emitter, $c\tau_E$.

3.3 *Extrapolation of RCLED design for enhancement of coherence-length range*

In the light of the analysis above, the theory also predicts the range of coherence-length variation that could be engineered. Planar microcavities clearly filter out inhomogeneous emission and this is likely to be effective until the spontaneous-emission lifetime is reached, which in these device could be as long as 10 ns. In principle, coherence lengths spanning five orders of magnitude could be accessed by increasing τ_c. To test this, consider increasing the cavity finesse, F, in the model for the devices discussed above. F is defined as the ratio of the cavity free spectral range, $\Delta\omega_{FSR}$, and the spectral width of a resonance, $\delta\omega$. Using the Fourier relationship with spectral width, the cavity coherence time, $\tau_c = 2/\delta\omega$, has a linear relationship with F given in Eq. (11).

$$F = \frac{\Delta\omega_{FSR}}{\delta\omega} \Rightarrow \tau_c = \frac{nL}{\pi c}F. \quad (11)$$

τ_c can also be related to the front and back mirror reflectivities, R_F and R_B, respectively, and the cavity length, L, by the expression

$$\tau_c = \frac{nL(1-\sqrt{R_F R_B})}{c\,[\sqrt{R_F R_B}]^{1/2}}. \quad (12)$$

The finesse may be varied by increasing the reflectivities of both device mirrors; however, the reader should note that in order to avoid lasing in high-finesse cavities, the gain must be reduced or the losses increased. Using gain and absorption estimates for these devices, the onset of lasing is likely to occur for $F > 500$.

Figure 4 shows the maximum and minimum coherence lengths for the useful NAs of the RCLED device as a function of finesse and for a range of device tunings. Here, a *useful* NA is where at least 10% of the device's power, emitted into air, is sampled and where coupling optics are effective set at an angle of 60°. An illustration of the useful NA is shown in the top left corner of Fig. 4.

Despite the restrictions on NA, a large variation in coherence length is apparent in this extrapolated example. Increasing the finesse by an order of magnitude increases the maximum coherence length by just over a factor of four. The minimum coherence length increases by nearly a factor of two. The range of coherence lengths, on the other hand, ranges from 10–20 to 20–80 μm, approaching a factor of five variation. The reader will also notice that a tuned microcavity device provides the greatest coherence-length range over useful NAs.

4 Conclusions

In summary, the coherence of planar microcavity devices is dependent on the underlying coherences of the cavity and emitter. This has been demonstrated by comparing derived analytical expressions for the coherence of planar microcavities with experimental results of measurement on RCLEDs. Here, the underlying statistical fluctuations of excitons of a quantum-well light source were exposed when

varying the NA. At low NAs, the coherence length is close to that of the bare microcavity. At large NAs, the coherence length is closer to that of the underlying emitter. A key aspect of the modelling shows that the coherence properties of planar microcavities can be engineered through microcavity design and selection of an emitter with suitable coherence properties.

ACKNOWLEDGEMENTS This work is supported by the Ultrafast Photonics Consortium (GR/R55078). Thanks are due to Dr. Jonathan Gray for experimental data and to Dr. Ricardo Coutinho and David Selviah for useful discussions.

REFERENCES

1 G. Björk, H. Heitmann, Y. Yamamoto, Phys. Rev. A **47**, 4451 (1993)
2 E.F. Schubert, Y.-H. Wang, A.Y. Cho, L.-W. Tu, G.J. Zydzik, Appl. Phys. Lett. **60**, 921 (1992)
3 H. Benisty, H. de Neve, C. Weisbuch, IEEE J. Quantum Electron. **34**, 1612 (1998)
4 E. Moreau, I. Robert, J.M. Gérard, I. Abram, L. Manin, V. Thierry-Mieg, Appl. Phys. Lett. **79**, 2865 (2001)
5 C. Santori, D. Fattal, J. Vučković, G.S. Solomon, Y. Yamamoto, Nature **419**, 594 (2002)
6 P.N. Stavrinou, M. Whitehead, C.C. Button, G. Parry, J. Appl. Phys. **86**, 3475 (1999)
7 R.F. Oulton, J.W. Gray, P.N. Stavrinou, G. Parry, Opt. Commun. **195**, 327 (2001)
8 R.C. Coutinho, D.R. Selviah, R.F. Oulton, J.W. Gray, P.N. Stavrinou, H.D. Griffiths, G. Parry, J. Lightwave Technol. **21**, 149 (2003)
9 R.H. Birkner, J. Kaiser, W. Elsäßer, C. Jung, Appl. Phys. B **79**, 963 (2004)
10 J. Heagerty, M.D. Sturge, J. Opt. Soc. Am. B **2**, 1143 (1985)
11 S. Schmit-Rink, D.S. Chemla, D.A.B. Miller, Adv. Phys. **38**, 89 (1989)
12 J.M. Schmitt, IEEE J. Sel. Top. Quantum Electron. **5**, 1205 (1999)
13 R.C. Youngquist, S. Carr, D. Davies, Opt. Lett. **12**, 158 (1987)
14 G.S. Kino, S.S.S. Chim, Appl. Opt. **29**, 3775 (1990)
15 M. Born, E. Wolf, *Principles of Optics*, 6th corrected edn. (Cambridge, Cambridge University Press, 1999)
16 K.H. Drexhage, in *Progress in Optics*, vol. 12, ed. by E. Wolf (North-Holland, Amsterdam, 1974), Chap. 6
17 D.G. Deppe, C. Lei, C. Lin, D.L. Huffaker, J. Mod. Opt. **41**, 325 (1994)